GEOPHYSICS, VOL. 69, NO. 1 (JANUARY-FEBRUARY 2004); P. 191–199, 15 FIGS.
10.1190/1.1649387

Estimating depth and model type using the continuous wavelet transform of magnetic data

Marc A. Vallée*, Pierre Keating‡, Richard S. Smith**, and Camille St-Hilaire*

ABSTRACT

The continuous wavelet transform has been proposed recently for the interpretation of potential field anomalies. Using Poisson wavelets, which are equivalent to an upward continuation of the analytic signal, this technique allows one to estimate the depth of burial of homogeneous field sources and to determine the nature of the source in the form of a structural index. Moreau et al. (1999) accomplish this by successively testing the least-squares misfit on a log–log plot of the wavelet transform amplitude versus the sum of the depth and the dilation (upward continuation height). We extend this methodology by analyzing the ratio of the Poisson wavelet coefficients of the first and second orders. For simple pole sources, this ratio at one dilation is enough to estimate the depth and index uniquely; but for extended sources of finite size, we must analyze the variation of the estimates with dilations. The technique gives good results on synthetic and field examples.

INTRODUCTION

The interpretation of potential field data is not a straightforward process because of the many of models capable of explaining the observed field. For this reason, the interpretation method selected must relate to the geology. Furthermore, if we wish to design an automatic interpretation technique that is to be applied over a large area with many anomalies, we prefer the model to be as simple as possible. Of currently available methods, Euler deconvolution (Thompson, 1982) is popular for automatic interpretation. This method assumes that the potential field $f(x, y, z)$ above a source is homogeneous of degree n and therefore satisfies (Thomson, 1982)

$$f(tx, ty, tz) = t^n f(x, y, z), \tag{1}$$

where t is an arbitrary constant. The value $N = -n$ is called the structural index and depends on the geometry of the source body.

Ridsdill-Smith and Dentith (1999) have developed the application of the wavelet transform for processing aeromagnetic data. With a specific family of wavelets, Hornby et al. (1999) analyze potential field data to locate singular features of the source distribution. Using the same family of wavelets, Moreau et al. (1997, 1999), Sailhac et al. (2000), and Martelet et al. (2001) develop another interpretation technique based on continuous wavelet theory. Their technique can estimate the source location and type, assuming the sources are homogeneous. The depth and structural index are estimated by successively testing the least-squares misfit between a straight line and the wavelet coefficients plotted against the dilation in log–log space. This technique, developed for homogeneous sources, has been generalized to multiple sources and extended sources of finite size and dipping angles (finite step, thin and thick dikes, prisms) by Sailhac et al. (2000), Martelet et al. (2001), and Sailhac and Gibert (2003).

We propose an alternative technique that estimates the depth and the structural index from the ratio of wavelets of successive orders. We show how to interpret these results over multiple (nonhomogeneous) sources, such as a finite step, and thin and thick dikes. This method is an extension of the technique of Hsu et al. (1998) and Sailhac et al. (2000), who both consider cases of extended sources with one finite dimension such as thin dikes of finite depth extent and thick dike models. These authors also discuss the influence of variable dip angle of the sources and show how to estimate the finite size of some sources. When wavelets or upward continuation is used, there is a lack of resolution that can be considered as a limitation compared to the technique of Hsu et al. (1998). Moreau et al. (1999), Sailhac (1999), and Martelet et al. (2001) show how this can be useful with regard to S/N ratio. Our method could potentially be generalized to three dimensions using the developments proposed by Sailhac and Gibert (2003).

Published on Geophysics Online September 18, 2003. Presented at the 72nd Annual Meeting, Society of Exploration Geophysicists. Manuscript received by the Editor March 21, 2003; revised manuscript received August 19, 2003.
*Fugro Airborne Surveys, 5610, Chemin Bois-Franc, St-Laurent, Montreal, Quebec H4S 1A9, Canada. E-mail: mvalle@fugroairborne.com; csthilaire@fugroairborne.com.
‡Geological Survey of Canada, 615 rue Booth, Ottawa, Ontario K1A 0E9, Canada. E-mail: pkeating@nrcan.gc.ca.
**Fugro Airborne Surveys, 2060 Walkley Road, Ottawa, Ontario K1G 3P5, Canada. E-mail: rsmith@fugroairborne.com.

METHODOLOGY

We recall the theory developed by Moreau et al. (1997, 1999), and Sailhac (1999), applied in a 2D physical space. The continuous wavelet transform W of a measured potential $\phi_0(x)$ is defined as

$$W_{\psi|\phi_0}(b,a) = \int_{-\infty}^{+\infty} \frac{dx}{a}\psi\left(\frac{b-x}{a}\right)\phi_0(x) = (D_a\psi * \phi_0)(b), \quad (2)$$

where ψ is the analyzing wavelet, b is a position parameter, a is a dilation parameter, and the dilation operator D_a is defined by

$$D_a\psi(x) = \frac{1}{a}\psi\left(\frac{x}{a}\right). \quad (3)$$

Moreau et al. (1997, 1999) show that a special class of wavelets is obtained when a homogeneous Fourier multiplier of degree γ (equivalent to a derivative of order γ) and a dilation are applied to the Poisson semigroup kernel. This kernel actually defines the continuation filter $P_a(x)$, which transforms the harmonic field from the measured level z to the level $z+a$:

$$P_a(x) = \frac{1}{\pi}\frac{a}{(a^2+x^2)}. \quad (4)$$

Horizontal and vertical wavelets are defined as

$$\psi_x^\gamma(x) = \frac{\partial^\gamma}{\partial x^\gamma}\left[\frac{1}{\pi}\frac{1}{(1+x^2)}\right] \quad (5)$$

and

$$\psi_z^\gamma(x) = \frac{\partial^{\gamma-1}}{\partial x^{\gamma-1}}\frac{\partial}{\partial a}\left[\frac{1}{\pi}\frac{a}{(a^2+x^2)}\right]\Bigg|_{a=1}, \quad (6)$$

with γ being the order of the analyzing wavelet. A complex wavelet is defined as (Moreau, 1995)

$$\psi_c^\gamma(x) = \psi_x^\gamma(x) - i\psi_z^\gamma(x). \quad (7)$$

The complex wavelet coefficients are associated with the upward-continued analytic signal amplitude A_n introduced by Nabighian (1972) and generalized by Hsu et al. (1996) as

$$A_n = \frac{\partial^n}{\partial x^n}\left(\frac{\partial}{\partial x}\phi\right) + i\frac{\partial^n}{\partial x^n}\left(\frac{\partial}{\partial z}\phi\right). \quad (8)$$

The specific relationship is (Sailhac et al., 2000)

$$\left|W_{\psi^\gamma|\phi(.,z=0)}(x,a)\right| = a^\gamma|A_{\gamma-1}|. \quad (9)$$

The modulus of the wavelet coefficients of order γ at dilation a is proportional to the modulus of the upward-continued complex analytic signal of order $\gamma-1$. For the class of wavelets previously defined, Moreau et al. (1997, 1999) show that, over a homogeneous source located at $x=0$, $z=z_0$ with a structural index $N=-n$, the following equation relates the wavelet coefficients at two levels, a and a':

$$W_{\psi^\gamma|\phi(.,z=0)}(x,a) = \left(\frac{a}{a'}\right)^\gamma\left(\frac{a'+z_0}{a+z_0}\right)^{-\beta} \times W_{\psi^\gamma|\phi(.,z=0)}\left(x\frac{a'+z_0}{a+z_0}, a'\right), \quad (10)$$

where

$$\beta = -(\gamma+N). \quad (11)$$

Moreau et al. (1997) propose estimating the source depth from the intersection of the lines of maxima of the wavelet transform, where the noise is minimized. These maxima also coincide with constant-phase wavelet transforms. Another approach suggested by Moreau et al. (1999) and Sailhac et al. (2000) is to estimate the source depth by finding the depth for which $\log(W_a/a^\gamma)$ varies linearly with increasing $\log(a+z_0)$. In practice, this is done by fitting a straight line to the plot of $\log(W_a/a^\gamma)$ versus $\log(a+z_0)$ and looking for the best least-squares fit which provides z_0. These techniques assume a simple (local homogeneous) source, and the analysis is generally done using the first-order $\gamma=1$ wavelet coefficients.

For multiple or extended sources (sources that are not homogeneous), e.g., the finite step model, this approach cannot be used because the log–log plot exhibits a curved shape with a linear tendency only at very high dilations. Based on this observation, Martelet et al. (2001) propose a modification to the original technique: starting from the entire range of dilations, they successively test the least-squares misfit between the log–log plot and its linear fit over a series of decreasing dilation ranges. They select only the dilation range for which the variance of the misfit is a minimum for the depth estimation. Over finite sources, Sailhac et al. (2000) propose the so-called function $H(a)$, generalized to three dimensions by Sailhac and Gibert (2003) to the function $S2(a)$.

We propose an alternative approach for estimating the depth of homogeneous sources. Our approach parallels that of Smith et al. (1998), who use higher order derivatives to determine the model type or the structural index. In the context of wavelets, this is comparable to using the ratio of the second to the first order wavelet coefficients. We define the ratio of wavelet transforms of successive orders $r^\gamma(x,a)$ as

$$r^\gamma(x,a) = \frac{1}{a}\frac{W_{\psi^{\gamma+1}|\phi(.,z=0)}(x,a)}{W_{\psi^\gamma|\phi(.,z=0)}(x,a)}. \quad (12)$$

This approach can be compared to the ratio of the analytic signal of successive orders defined by Hsu et al. (1998). Furthermore, we define the ratio R for different dilations a and a' and positions x and x' as

$$R = \frac{r^\gamma(x,a)}{r^\gamma(x',a')}. \quad (13)$$

For a homogeneous source located at $z=z_0$, the phase of $W_{\psi^\gamma|\phi(.,z=0)}(x',a')$ is the same as that of $W_{\psi^\gamma|\phi(.,z=0)}(x,a)$, with $x'=x[(a'+z_0)/(a+z_0)]$; thus, we can apply equation (10) and derive

$$R = \frac{a'}{a}\frac{W_{\psi^{\gamma+1}|\phi(.,z=0)}(x,a)}{W_{\psi^\gamma|\phi(.,z=0)}(x,a)}\frac{W_{\psi^\gamma|\phi(.,z=0)}\left(x\frac{a'+z_0}{a+z_0}, a'\right)}{W_{\psi^{\gamma+1}|\phi(.,z=0)}\left(x\frac{a'+z_0}{a+z_0}, a'\right)} = \frac{a'+z_0}{a+z_0}. \quad (14)$$

From this equation, we define the source depth estimator as

$$z_0(a,a') = \frac{a'-aR}{R-1}, \quad (15)$$

and the structural index estimator by combining equations (10), (11), and (14):

$$N(a,a') = \frac{\log\left[\left(\frac{a'}{a}\right)^{\gamma}\frac{W_{\psi^\gamma|\phi(.,z=0)}(x,a)}{W_{\psi^\gamma|\phi(.,z=0)}(x',a')}\right]}{\log(R)} - \gamma. \quad (16)$$

Moreau (1995) introduces similar relations to estimate the depth and structural index from the ratio of wavelet moduli at different scales a and a'. In practice, our analysis is done by using the first-order $\gamma = 1$ and second-order $\gamma = 2$ wavelet coefficients. For homogeneous sources, the first- and second-order maxima coincide, respectively, with constant-phase wavelet transforms, and the ratio of wavelet transforms coincides with the ratio of their modulus. This technique allows the estimation of the depth and structural index for any dilation pair. For a homogeneous model, using a different dilation pair gives the same depth and structural index. The solution is derived for an infinite step (contact) in Appendix A and a vertical thin dike in Appendix B. The estimated depth and structural index are constant at all dilations. However, for an extended source, this is not the case, as shown later.

Summary of the implementation

We propose an implementation of this algorithm that includes the following steps:

1) Start with a magnetic field profile.
2) Extend the profile prior to the Fourier transform.
3) Fourier transform the extended profile.
4) In the wavenumber domain, compute the Fourier transform of the horizontal and vertical derivatives.
5) In the wavenumber domain, compute the Fourier transform of the upward-continued derivatives for several dilations (heights). The choice of the dilations is discussed in the presentation of the first model example.
6) Transform to the space domain the first- and second-order derivatives for successive heights.
7) Compute the analytic signal of orders 0 and 1 and normalize by the dilations to obtain the wavelet transforms.
8) Search for the maxima along the wavelet coefficient profiles and find the associated maxima for successive heights.
9) Apply equations (12), (13), (15), and (16) to estimate the depth and structural index from different pairs of dilations. The choice of dilations for the finite vertical step model is discussed below.
10) Select the best estimates for the variation of the estimates with dilations. The details of this step are discussed in the presentation of the field example.

EXTENDED MODEL EXAMPLES

We illustrate the application of equations (15) and (16) to the response of three synthetic extended models: the finite vertical step, the finite vertical sheet, and the infinite vertical thick dike. The mathematical derivations are given in Appendices C, D, and E, respectively.

Vertical step

The finite vertical step model, located at x_1 with upper and lower depths z_1 and z_2, is illustrated in Figure 1. The source depth and structural index predicted by our method from the analytic solution of the upward-continued derivatives, as derived in Appendix C, are obtained from

$$z_0(a,a') = \frac{a'(z_{12}+a')(z_1+a)(z_2+a) - a(z_{12}+a)(z_1+a')(z_2+a')}{(z_{12}+a)(z_1+a')(z_2+a') - (z_{12}+a')(z_1+a)(z_2+a)}, \quad (17)$$

and

$$N(a,a') = \frac{\log\left[\frac{(z_1+a')(z_2+a')}{(z_1+a)(z_2+a)}\right]}{\log(R)} - 1, \quad (18)$$

where $z_{12} = (z_1+z_2)/2$ and

$$R = \frac{(z_{12}+a)(z_1+a')(z_2+a')}{(z_{12}+a')(z_1+a)(z_2+a)}. \quad (19)$$

The successive dilations a and a' appear as ratios in equations (17)–(19), and it seems reasonable to study the solutions as a function of the ratio a'/a. This suggests plotting the depth and structural index versus the lower dilation a using a logarithmic scale for dilation. The solutions for a step with $z_1 = 100$ m and $z_2 = 400$ m ($z_2/z_1 = 4$) are presented in Figures 2 and 3 for different ratios of a'/a. Similar curves are observed for these different ratios, except that the best resolution is obtained for the lowest ratio $a'/a = \sqrt[4]{2} = 1.19$. This dilation ratio is used in the remaining presentations of this paper.

The solutions for a step with $z_1 = 100$ m are presented in Figures 4 and 5. When the ratio z_2/z_1 is close to 1, the structural index is near 1, which is the structural index of a magnetic horizontal thin sheet. As the ratio z_2/z_1 increases, the solution asymptotically approaches two limits, one for low dilations and one for high dilations, as observed by Sailhac et al. (2000). The

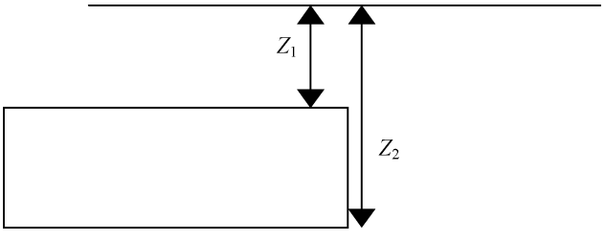

FIG. 1. Vertical step model with depths to top z_1 and bottom z_2.

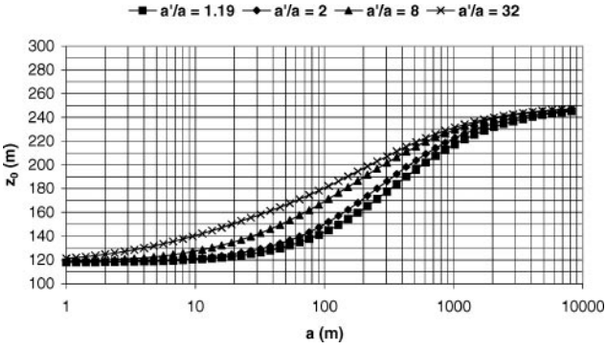

FIG. 2. Predicted depth from analytic solution of a vertical step with various ratios of a'/a and $z_2/z_1 = 4$, z_1 being at 100 m.

low-dilation solutions converge to a depth near z_1 and a structural index near 0 (magnetic contact), and the high-dilation solutions converge to a depth of z_{12} and a structural index of 1 (magnetic thin sheet).

At low dilations, which means the observations are very close to the source, the algorithm responds mostly to the depth to the top. The structural index N is near 0 because the step is seen with apparent infinite vertical extent. At very large dilations, that is, very far from the source $z_{12} + a \gg (z_2 - z_1)/2$, the algorithm responds to a thin sheet-like source approximation of the extended body (which is why the depth converges to z_{12}). The value N is near 1 because the step is seen as a horizontal thin sheet. Between these two extremes, the plot provides little interpretable information. More importantly, the information at low dilations must be treated very carefully. Such information will give reliable results on the depth to the top only if the source is quite shallow—that is, only if z_1 is relatively small. For larger z_1 (that is, for deeper sources), z_2/z_1 would tend to 1, the profile would be flatter, and it would stay closer to the z_{12} value even for small dilations.

The fundamentally weaker reliability of the low-dilation calculation is confirmed by the poorly resolved structural index in Figure 3. The higher we are from the source, the more reliable the structural index calculation is. Also, for any finite source, the structural index at large dilation is always equivalent to that of the point source and is more stable. This observation is analyzed by Poulet et al. (2001). However, as they point out, when a single anomaly is analyzed, there is a practical limitation in the maximum dilation that can be used as a result of the interference of nearby anomalies. Furthermore, the upward continuation process distorts the anomalies near the edges of the profile, as a result of extending the data and the assumed periodicity inherent in the Fourier transform.

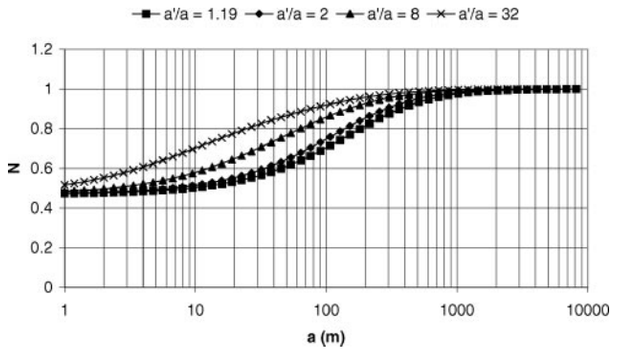

FIG. 3. Predicted structural index from analytic solution of a vertical step with various ratios of a'/a and $z_2/z_1 = 4$, z_1 being at 100 m.

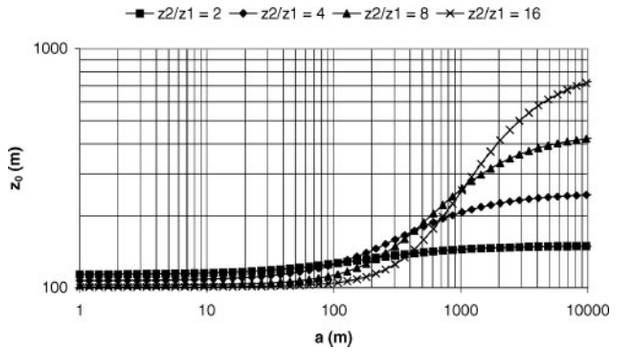

FIG. 4. Predicted depth from analytic solution of a vertical step with various ratios of z_2/z_1, z_1 being at 100 m; $a'/a = 1.19$.

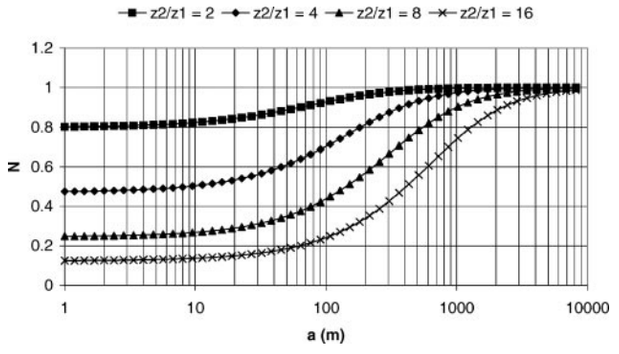

FIG. 5. Predicted structural index from analytic solution of a vertical step with various ratios of z_2/z_1, z_1 being at 100 m; $a'/a = 1.19$.

Vertical thin dike

The finite vertical dike model located at x_0 with depths to the top and bottom of z_1 and z_2, respectively, is illustrated in Figure 6. The source depth and structural index predicted by our method from the analytic solution of the upward continuation are given in Appendix D. The solutions for a dike with $z_1 = 100$ m are presented in Figures 7 and 8. The shapes of the solutions are similar to the shape of the solutions for a finite

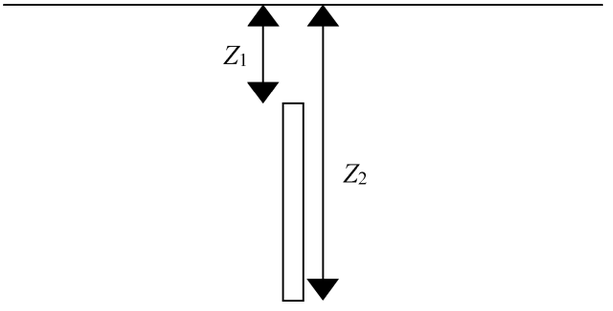

FIG. 6. Finite vertical dike model with depths to top z_1 and bottom z_2.

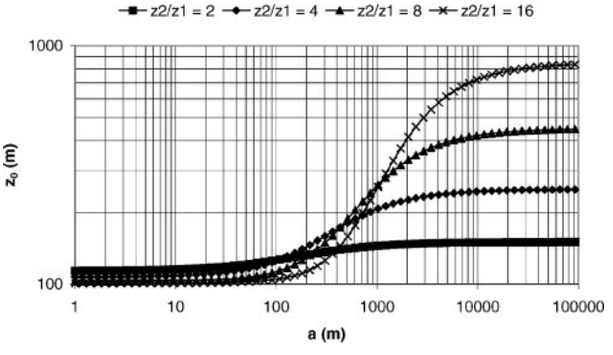

FIG. 7. Predicted depth from analytic solution of a vertical dike with various ratios of z_2/z_1, z_1 being at 100 m; $a'/a = 1.19$.

step except for the structural indices, which vary between 1 and 2 for the low and high dilation limits, respectively.

Vertical thick dike

The vertical thick dike model with a width $2t$ and depth-to-top z_1 illustrated in Figure 9, is a special case of the prism model presented by Sailhac et al. (2000). Its analytic signal is studied by Hsu et al. (1998), who show there are important differences when the half-thickness t is larger or smaller than the depth z_1: when the half-thickness is larger than the depth, the analytic signal has two peaks, located at

$$x = \pm\sqrt{t^2 - z_1^2} \tag{20}$$

(see Figure 10). As dilation increases, the two peaks converge to one peak, located at the center of the dike. The source depth and structural index predicted by our method from the analytic solution of the upward-continued derivatives of a thick dike are derived in Appendix E and shown in Figures 11 and 12. At low dilations, the predicted depth is several orders of magnitude larger than the real depth to top but converges to the depth to top as the scale a increases. The predicted structural index is around 3.7 at a dilation of 500 but converges at large dilations to a structural index of 1, which is the correct structural index of a dike.

When depth and structural index are estimated from profile data (measured or synthetic) from numerical estimation of the upward-continued derivatives, there is a practical limitation in the maximum dilation that can be used. This can be observed in Figures 11 and 12, where the depth and the structural index estimated over a synthetic anomaly by applying the wavelet transform are compared with the depth and the structural index predicted analytically. The predicted and estimated curves agree for small scales but start diverging for $a > 1000$. Another limitation comes from nearby anomalies, which is in this case a result of computing the wavelet transform by Fourier transform.

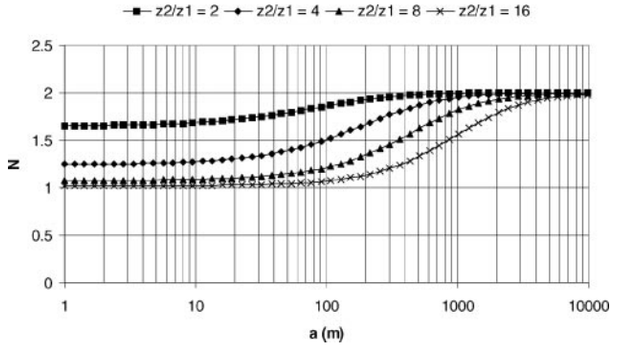

FIG. 8. Predicted structural index from analytic solution of a vertical dike with various ratios of z_2/z_1, z_1 being at 100 m; $a'/a = 1.19$.

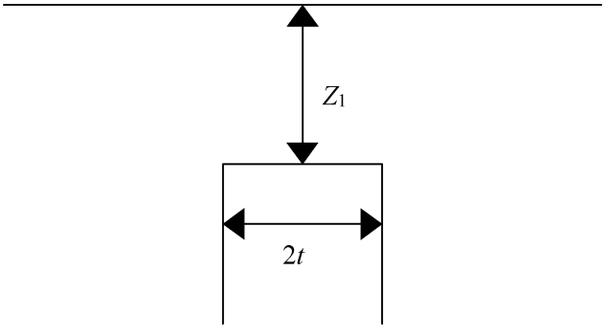

FIG. 9. Thick dike model with depth z_1 and half-thickness t.

FIELD EXAMPLE

We test the proposed technique on profile data from an area located in northeastern Ontario, Canada. The region is within the Abitibi subprovince, which has a general east–west strike and includes many elongated volcanic bands and large granitic

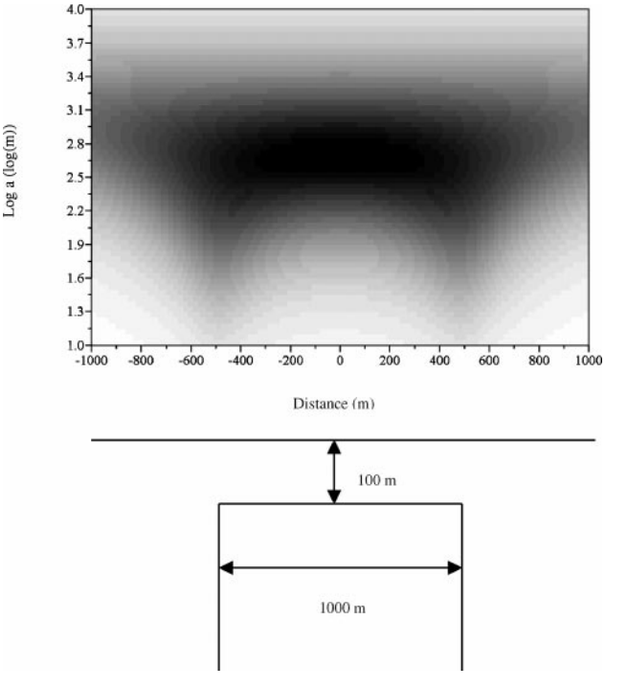

FIG. 10. Plot of the amplitude of the wavelet coefficient computed above a thick dike. Dark areas show maxima in the amplitude. At low dilations, two peaks are located above the edges of the dike. At high dilation, a single peak is located above the center of the dike.

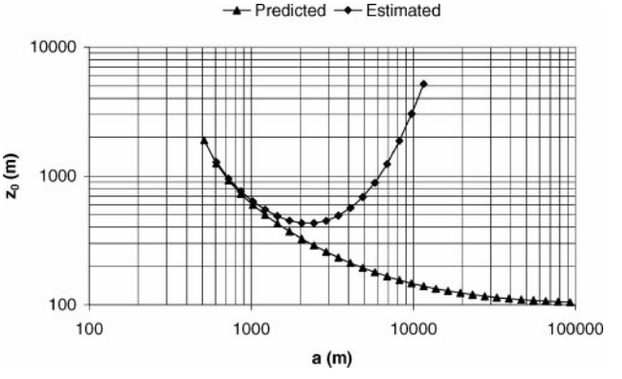

FIG. 11. Predicted depth from analytic solution and estimated depth from a profile over a vertical thick dike located at 100 m depth with a thickness of 1000 m. The anomaly is sampled over a length of 20 km; $a'/a = 1.19$.

intrusions. It is well known for its mineral potential and has been extensively explored. Drill-hole data (OGS, 1999) are available and can be used to determine depth to bedrock in some areas. Although over one thousand boreholes are available, they tend to be concentrated along specific geological horizons such as the Pocupine-Destor fault zone. Much of the region is covered by glacial drift, and in some areas outcrops are very scarce. Overburden thickness averages 35 m (Jensen et al., 1985) and can be in excess of 50 m, thereby rendering geological mapping very difficult. The area is of interest because of the many gold deposits in the area. As well, a number of dike swarms are in the area, including a set of east–west diabase dikes.

Geophysical data are from a combined magnetic-electromagnetic survey (OGS, 2000) flown at 200-m line spacing in a N30°W direction perpendicular to the main geological strike of the area. The magnetic sensor was located in a bird about 70 m above ground. The sampling interval along the flight lines was 12 m on average. Part of line 81921 contains an anomaly located at a distance of 18 180 m along the profile shown in Figures 13 and 15. This anomaly is associated with a mapped bedrock diabase dike. A borehole is located nearby and intersects the bedrock at 41 m.

The estimation of the depth and structural index of this source is shown in Figure 14. The curves show a plateau at low dilations, then a drop of the two parameters at large dilations. This behavior is similar to the case of a thick vertical dike (Figures 11 and 12). However, in this case there is variability at large dilations, probably from interference from adjacent anomalies. Our strategy is to use the value at the dilation where the estimates change most slowly with changing dilation. In Figure 14, this occurs at the plateau at dilations of about 15 m, where the estimated depth is 145 m and the structural index is 1.2. An index close to 1 implies a thin dike model. The synthetic response of a 17-m thin dike model with a depth to top of 145 m and a susceptibility of 0.4327 SI is computed and plotted in Figure 15, where there clearly is close agreement with the measured data.

CONCLUSIONS

An alternative method has been proposed to estimate the depth and structural index of magnetic sources using the wavelet transform. Estimates can be obtained from the ratios of normalized analytic signals at two altitudes and two orders of derivation. The proposed method has been tested over synthetic and field data. A numerical model confirms the interpretation of the field data. This method is easy to implement

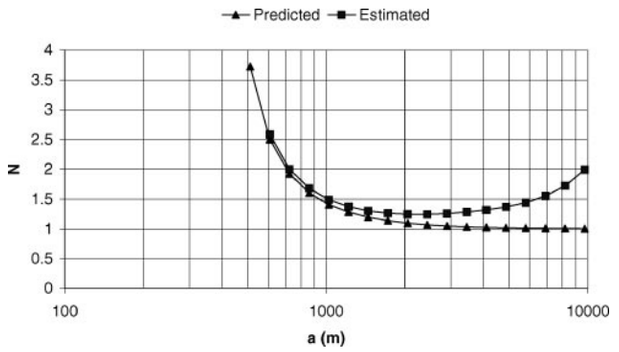

FIG. 12. Predicted structural index from analytic solution and estimated structural index from a profile over a vertical thick dike located at 100 m depth with a thickness of 1000 m. The anomaly is sampled over a length of 20 km; $a'/a = 1.19$.

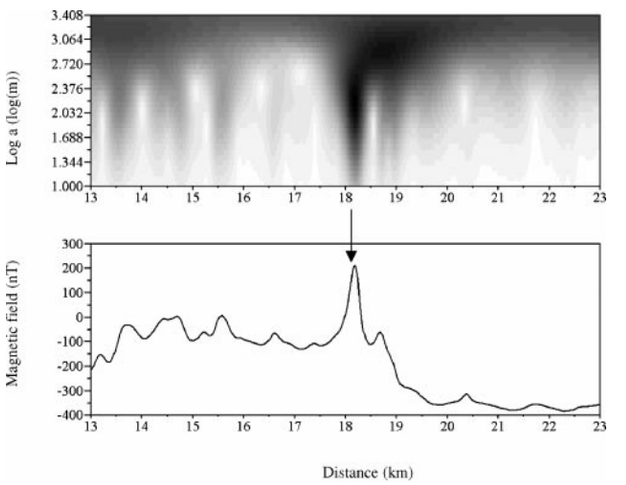

FIG. 13. Total magnetic field along a portion of line 81921. The amplitude of the first-order wavelet transform coefficients is in the top panel. The dark areas indicate maxima of the wavelet coefficient. The arrow indicates the location of the anomaly studied.

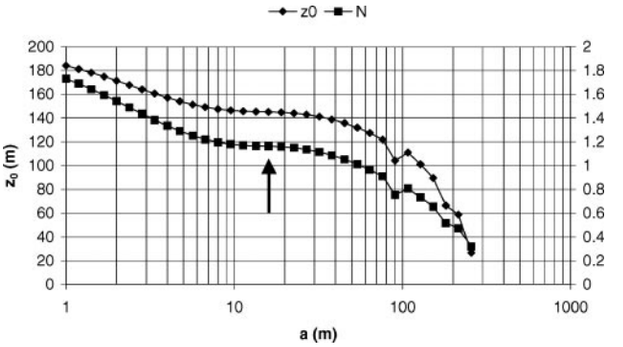

FIG. 14. Estimated depth $z_0(a, a')$ and structural index $N(a, a')$ for the anomaly presented in Figure 13; $a'/a = 1.19$. The arrow indicates the estimated depth and structural index.

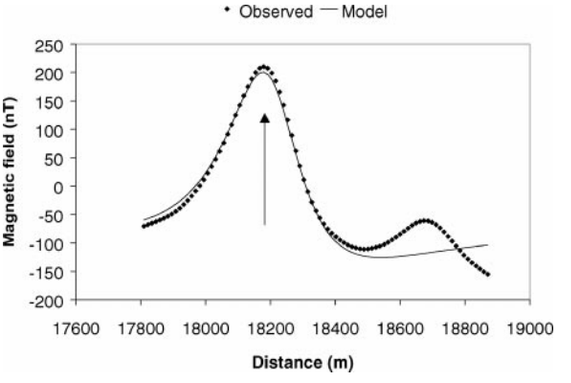

FIG. 15. Total magnetic field along a portion of line 81921. The field produced by a 17-m-wide dike located 145 m below the sensor extending to 500 m depth is superimposed. The arrow indicates the location of the anomaly studied.

in a computer program and should improve estimates over extended sources. The method potentially could be generalized to three dimensions using the developments proposed by Sailhac and Gibert (2003).

ACKNOWLEDGMENTS

We thank Fugro Airborne Surveys for supporting this research. Constructive reviews from A. H. Saad, P. Sailhac, F. Boschetti, and T. Ridsdill-Smith greatly improved the original manuscript. This is GSC contribution 2003029.

REFERENCES

Hornby, P., Boschetti, F., and Horovitz, F. G., 1999, Analysis of potential field data in the wavelet domain: Geophysical Journal International, **137**, 175–196.

Hsu, S.-K., Coppens, D., and Shyu, C.-T., 1998, Depth to magnetic source using the generalized analytic signal: Geophysics, **63**, 1947–1957.

Hsu, S.-K., Sibuet, J.-C., and Shyu, C.-T., 1996, High-resolution detection of geologic boundaries from potential-field anomalies: An enhanced analytic signal technique: Geophysics, **61**, 373–386.

Jensen, L. S., Baker, C. L., and Trowell, N. F., 1985, Preliminary results of bedrock samples from sonic drilling program in the Matheson area, Cochrane District, map P. 2848, scale 1:100 000: Ontario Geological Survey.

Martelet, G., Sailhac, P., Moreau, F., and Diament, M., 2001, Characterization of geological boundaries using 1-D wavelet transform on gravity data: Theory and application to the Himalayas: Geophysics, **66**, 1116–1129.

Moreau, F., 1995, Méthodes de traitement de données géophysiques par transformée en ondelettes: Ph.D. thesis, Univ. de Rennes I.

Moreau, F., Gibert, D., Holschneider, M., and Saracco, G., 1997, Wavelet analysis of potential fields: Inverse Problems, **13**, 165–178.

——— 1999, Identification of sources of potential fields with the continuous wavelet transform: Basic theory: Journal of Geophysical Research, **104**, 5003–5013.

Nabighian, M. N., 1972, The analytic signal of two-dimensional magnetic bodies with polygonal cross-section: Its properties and use for automated anomaly interpretation: Geophysics, **37**, 507–517.

Ontario Geological Survey, 1999, The Ontario drill hole database: ERLIS data set 13.

——— 2000, Ontario airborne geophysical surveys, magnetic and electromagnetic data, Matheson area: Geophysical data set 1101.

Poulet, T., D'Escrivan, H., Boschetti, F., Hornby, P., and Horowiz, F., 2001, New advances in the analysis of potential field data by multiscale edges: 15th Geophysical Conference and Exhibition, Australian Society of Exploration Geophysicists, Proceedings.

Ridsdill-Smith, T. A., and Dentith, M. C., 1999, The wavelet transform in aeromagnetic processing: Geophysics, **64**, 1003–1013.

Sailhac, P., 1999, Analyse multiéchelle et inversion de données géophysiques en Guyane Française: Ph. D. thesis, Institut de Physique du Globe de Paris.

Sailhac, P., and Gibert, D., 2003, Identification of sources of potential fields with the continuous wavelet transform: 2D wavelets and multipolar approximations: Journal of Geophysical Research, **108**, 2296–2306.

Sailhac, P., Galdeano, A., Gibert, D., Moreau, F., and Delor, C., 2000, Identification of sources of potential fields with the continuous wavelet transform: Complex wavelets and application to aeromagnetic profiles in French Guiana: Journal of Geophysical Research, **105**, 19455–19475.

Smith, R. S., Thurston, J. B., Dai, T.-F., and MacLeod, I. N., 1998, iSPI™—The improved source parameter imaging method: Geophysical Prospecting, **46**, 141–151.

Thompson, D. T., 1982, EULDPH—A new technique for making computer-assisted depth estimates from magnetic data: Geophysics, **47**, 31–37.

APPENDIX A

WAVELET TRANSFORM SOLUTIONS OF AN INFINITE STEP (CONTACT)

Estimates of the depth and structural index can be derived from the analytic solution of a potential field. The top of the vertical step is located at x_1 and depth z_1. The complex analytic signal of the magnetic field was first introduced by Nabighian (1972). The analytic signal of the total magnetic field of a vertical infinite step is the following function of the variable $w = x + iz$:

$$A_0(w) = \frac{\alpha e^{i\theta}}{w - w_1}, \tag{A-1}$$

where $\alpha = 2KFc$, in which K is the susceptibility contrast at the contact, F is the magnitude of the earth's magnetic field, $c = 1 - \cos^2 i \sin^2 A$, and A is the angle between the positive x-axis and magnetic north; i is the ambient-field inclination; $\tan I = \tan i / \cos A$; and $\theta = 2I + 90$. Note that θ differs by 270° from ϕ defined by Nabighian (1972). This is because we multiply the numerator and denominator in Nabighian's equation by $-i = \exp(3\pi i/2)$ to simplify equation (A-1).

At $x = x_1 = 0$, the first-order wavelet transform modulus can be obtained from equations (9) and (A-1), giving

$$\left|W_{\psi_c^1|\partial T(.,z=0)}(0, a)\right| = \frac{\alpha a}{(z_1 + a)}. \tag{A-2}$$

For the same model, the analytic signal of the first order obtained from applying equation (8) on equation (A-1) is

$$A_1(w) = \frac{-\alpha e^{i\theta}}{(w - w_1)^2}. \tag{A-3}$$

The second-order wavelet transform modulus is

$$\left|W_{\psi_c^2|\partial T(.,z=0)}(0, a)\right| = \frac{\alpha a^2}{(z_1 + a)^2}. \tag{A-4}$$

Applying equation (14), we find the dilation ratio as

$$R = \frac{(z_1 + a')}{(z_1 + a)}. \tag{A-5}$$

From equations (15) and (16), the depth estimate is $z_0(a, a') = z_1$ and the structural index is $N(a, a') = 0$.

APPENDIX B

WAVELET TRANSFORM SOLUTIONS OF AN INFINITE THIN SHEET

The total field anomaly of the vertical thin sheet is the horizontal derivative of the vertical contact (Nabighian, 1972), and the analytic signal is the horizontal derivative of equation (A-1), i.e.,

$$A_0(w) = \frac{-\alpha e^{i\theta}}{(w - w_1)^2}. \tag{B-1}$$

At $x = x_1 = 0$, the first-order wavelet transform modulus can be obtained from equations (9) and (B-1), giving

$$\left|W_{\psi_c^1|\partial T(.,z=0)}(0, a)\right| = \frac{\alpha a}{(z_1 + a)^2}. \tag{B-2}$$

For the same model, the analytic signal of the first order obtained from applying equation (8) on equation (B-1) is

$$A_1(w) = \frac{2\alpha e^{i\theta}}{(w - w_1)^3}. \quad \text{(B-3)}$$

The second-order wavelet transform modulus is

$$\left|W_{\psi_c^2|\partial T(.,z=0)}(0,a)\right| = \frac{2\alpha a^2}{(z_1 + a)^3}. \quad \text{(B-4)}$$

Applying equation (14), we find the dilation ratio:

$$R = \frac{(z_1 + a')}{(z_1 + a)}. \quad \text{(B-5)}$$

From equations (15) and (16), the depth estimate is $z_0(a, a') = z_1$ and the structural index is $N(a, a') = 1$.

APPENDIX C

WAVELET TRANSFORM SOLUTIONS OF A FINITE VERTICAL STEP

The geometry of a vertical step located at x_1 and depths z_1 and z_2 is illustrated in Figure 1. The analytic signal of a finite step is the sum of two infinite steps [equation (A-1)] of opposite signs:

$$A_0(w) = \alpha e^{i\theta}\left[\frac{1}{w - w_1} - \frac{1}{w - w_2}\right]. \quad \text{(C-1)}$$

At $x = x_1 = 0$, the first-order wavelet transform modulus can be obtained from equations (9) and (C-1), giving

$$\left|W_{\psi_c^1|\partial T(.,z=0)}(0,a)\right| = \frac{2\alpha a h}{(z_1 + a)(z_2 + a)}, \quad \text{(C-2)}$$

where $h = (z_2 - z_1)/2$. Equation (C-2) is a special case of the general solution developed by Sailhac et al. (2000) for an inclined magnetic step. For the finite vertical step, the first-order analytic signal is derived from applying equation (8) on equation (C-1):

$$A_1(w) = \alpha e^{i\theta}\left[\frac{1}{(w - w_2)^2} - \frac{1}{(w - w_1)^2}\right]. \quad \text{(C-3)}$$

The second-order wavelet transform modulus comes from equation (9):

$$\left|W_{\psi_c^2|\partial T(.,z=0)}(0,a)\right| = \frac{4\alpha a^2 h(z_{12} + a)}{(z_1 + a)^2(z_2 + a)^2}, \quad \text{(C-4)}$$

where $z_{12} = (z_1 + z_2)/2$. Because the phase is constant, we can apply equation (14) on the wavelet modulus. The dilation ratio is

$$R = \frac{(z_{12} + a)(z_1 + a')(z_2 + a')}{(z_{12} + a')(z_1 + a)(z_2 + a)}. \quad \text{(C-5)}$$

The source depth and structural index predicted by our method from the analytic solution of the upward-continued derivatives are obtained from substitution into equation (14):

$$z_0(a, a') = \frac{a'(z_{12} + a')(z_1 + a)(z_2 + a) - a(z_{12} + a)(z_1 + a')(z_2 + a')}{(z_{12} + a)(z_1 + a')(z_2 + a') - (z_{12} + a')(z_1 + a)(z_2 + a)}, \quad \text{(C-6)}$$

and

$$N(a, a') = \frac{\log\left[\dfrac{(z_1 + a')(z_2 + a')}{(z_1 + a)(z_2 + a)}\right]}{\log(R)} - 1. \quad \text{(C-7)}$$

APPENDIX D

WAVELET TRANSFORM SOLUTIONS OF A FINITE VERTICAL THIN SHEET

The geometry of a vertical dike located at $x = 0$ and extending from depth z_1 to depth z_2 is illustrated in Figure 4. The analytic signal of the finite vertical dike is the difference of two infinite dikes [equation (B-1)] at different depths, i.e.,

$$A_0(w) = \alpha e^{i\theta}\left[\frac{-1}{(w - w_1)^2} + \frac{1}{(w - w_2)^2}\right]. \quad \text{(D-1)}$$

At $x = x_1 = 0$, the first-order wavelet transform modulus is

$$\left|W_{\psi_c^1|\partial T(.,z=0)}(0,a)\right| = \frac{4\alpha a h(z_{12} + a)}{(z_1 + a)^2(z_2 + a)^2}. \quad \text{(D-2)}$$

Sailhac et al. (2000) present a general solution for an inclined dike. For the finite vertical thin sheet, the first-order analytic signal is found by applying equation (8) on equation (D-1):

$$A_1(w) = 2\alpha e^{i\theta}\left[\frac{1}{(w - w_1)^3} - \frac{1}{(w - w_2)^3}\right]. \quad \text{(D-3)}$$

The second-order wavelet transform modulus is

$$\left|W_{\psi_c^2|\partial T(.,z=0)}(0,a)\right| = \frac{4\alpha a^2 h\left(3a^2 + 3z_1 a + 3z_2 a + z_1^2 + z_2^2 + z_1 z_2\right)}{(z_1 + a)^3(z_2 + a)^3}. \quad \text{(D-4)}$$

Applying equation (14), we find the dilation ratio:

$$R = \frac{(z_{12} + a')(z_1 + a')(z_2 + a')\left(3a^2 + 3z_1 a + 3z_2 a + z_1^2 + z_2^2 + z_1 z_2\right)}{(z_{12} + a)(z_1 + a)(z_2 + a)\left(3a'^2 + 3z_1 a' + 3z_2 a' + z_1^2 + z_2^2 + z_1 z_2\right)}. \quad \text{(D-5)}$$

The source depth is obtained by applying equation (15). The structural index is estimated as

$$N(a, a') = \frac{\log\left[\dfrac{(z_{12} + a)(z_1 + a')^2(z_2 + a')^2}{(z_{12} + a')(z_1 + a)^2(z_2 + a)^2}\right]}{\log(R)} - 1. \quad \text{(D-6)}$$

APPENDIX E

WAVELET TRANSFORM SOLUTIONS OF A VERTICAL THICK DIKE

The geometry of a vertical dike located between $x \pm t$ and extending to infinity is illustrated in Figure 7. The modulus of the analytic signal is given by Hsu et al. (1998) as

$$|A_0(x)| = \frac{2\alpha t}{\sqrt{\left[z_1^2 + (x-t)^2\right]\left[z_1^2 + (x+t)^2\right]}}. \quad \text{(E-1)}$$

The modulus of the first-order analytic signal is (Hsu et al., 1998)

$$|A_1(x)| = \frac{4\alpha t\sqrt{x^2 + z^2}}{\left[z_1^2 + (x-t)^2\right]\left[z_1^2 + (x+t)^2\right]}. \quad \text{(E-2)}$$

At $x = 0$, applying equation (15), we find the dilation ratio:

$$R = \frac{(z_1 + a)\left[(z_1 + a')^2 + t^2\right]}{(z_1 + a')\left[(z_1 + a)^2 + t^2\right]}. \quad \text{(E-3)}$$

The structural index is

$$N(a, a') = \frac{\log\left[\dfrac{(z_1 + a')^2 + t^2}{(z_1 + a)^2 + t^2}\right]}{\log(R)} - 1. \quad \text{(E-4)}$$